JBC Papers in Press. Published on August 8, 2017 as Manuscript M117.782490
The latest version is at http://www.jbc.org/cgi/doi/10.1074/jbc.M117.782490

Postsynaptic density 95 (PSD-95) serine 561 phosphorylation regulates a conformational switch and bidirectional dendritic spine structural plasticity

Qian Wu[*,1,2], Miao Sun[*,1], Laura P. Bernard[1] and Huaye Zhang[1]

1. Department of Neuroscience and Cell Biology, Robert Wood Johnson Medical School, Rutgers, The State University of New Jersey, Piscataway, NJ 08854
2. Current address: Department of Neuroscience and Physiology, New York University School of Medicine, 550 First Ave, New York, NY, 10016.

* These authors contributed equally to this work.

Correspondence addressed to: Dr. Huaye Zhang, Department of Neuroscience and Cell Biology, Rutgers Robert Wood Johnson Medical School, 675 Hoes Lane West, Piscataway, NJ 08854. Email: huaye.zhang@rutgers.edu

Running title: PSD-95 Ser561 phosphorylation and structural plasticity

Abstract

PSD-95 is a major synaptic scaffolding protein that plays a key role in bidirectional synaptic plasticity, which is a process important for learning and memory. It is known that PSD-95 shows increased dynamics upon induction of plasticity. Yet the underlying structural and functional changes in PSD-95 that mediate its role in plasticity remain unclear. Here we show that phosphorylation of PSD-95 at Ser561 in its GK domain, which is mediated by the partitioning defective 1 (Par1) kinases, regulates a conformational switch and is important for bidirectional plasticity. Using a fluorescence resonance energy transfer (FRET) biosensor, we show a phosphomimetic mutation of Ser561 promotes an intramolecular interaction between GK and the nearby SH3 domain, leading to a closed conformation; while a non-phosphorylatable S561A mutation or inhibition of Par1 kinase activity decreases SH3-GK interaction, causing PSD-95 to adopt an open conformation. In addition, S561A mutation facilitates the interaction between PSD-95 and its binding partners. Fluorescence recovery after photobleaching (FRAP) imaging reveals the S561A mutant shows increased stability, while the phosphomimetic S561D mutation increases PSD-95 dynamics at the synapse. Moreover, molecular replacement of endogenous PSD-95 with the S561A mutant blocks dendritic spine structural plasticity during chemical long-term potentiation (LTP) and long-term depression (LTD). Endogenous Ser561 phosphorylation is induced by synaptic NMDA receptor activation, and the SH3-GK domains exhibit a Ser561 phosphorylation-dependent switch to a closed conformation during synaptic plasticity. Our results provide novel mechanistic insight into the regulation of PSD-95 in dendritic spine structural plasticity through phosphorylation-mediated regulation of protein dynamics and conformation.

Introduction

The ability for synapses to undergo dynamic rearrangements is important for cognitive processes such as learning and memory (1-5). On a cellular level, synaptic plasticity is reflected by changes in the number and size of dendritic spines, which are mushroom-shaped protrusions on neurons that receive most of the excitatory synaptic inputs in the CNS (6). Dendritic spines enlarge during long-term potentiation (LTP), which is a long-lasting increase in synaptic strength (7). Enlarged spines usually contain larger postsynaptic density (PSD), an electron-dense protein complex located underneath the postsynaptic membrane. Larger spines are also associated with increased surface expression of AMPA type glutamate receptors (AMPARs),

which mediates basal synaptic transmission at glutamatergic synapses (8). By contrast, dendritic spines shrink during long-term depression (LTD), which is a long-lasting decrease in synaptic strength. These shrunken spines have smaller PSD and reduced surface expression of AMPARs, leading to weaker synaptic transmission (9-11).

Synaptic plasticity requires the dynamic reorganization of the PSD protein scaffold. One of the key scaffolding proteins at the postsynapse is PSD-95, which is a membrane-associated guanylate kinase (MAGUK) family protein (12). PSD-95 plays a key role in synaptic plasticity, as its overexpression blocks LTP and facilitates LTD (13) while knockdown of PSD-95 decreases LTD (14,15). At the structural level, PSD-95 contains three PDZ domains on the N-terminus, followed by a Src-Homology 3 (SH3) domain and a guanylate kinase (GK) domain. The SH3 and GK domains form an intramolecular interaction with each other (16-18). This intramolecular interaction is important for PSD-95 function (19,20), and previously identified genetic mutations in discs large (Dlg), the Drosophila homolog of PSD-95, disrupt this interaction (16,21). However, it is unclear how the SH3-GK interaction is regulated under physiological conditions and how this interaction may contribute to synaptic plasticity.

We recently identified a phosphorylation site in the GK domain of PSD-95, Ser561, which is phosphorylated by the microtubule affinity regulating kinase (MARK)/partitioning defective 1 (Par1) family of kinases (22). Using pull-down and fluorescence resonance energy transfer (FRET) assays, we now show that Ser561 phosphorylation regulates a conformational switch in PSD-95 by promoting the intramolecular interaction between the SH3 and GK domains. In addition, we show that a non-phosphorylatable S561A mutation increases the interaction between PSD-95 and its binding partners. Using fluorescence recovery after photobleaching (FRAP) imaging, we further show that a phosphomimetic S561D mutation increases the dynamics of PSD-95 at the synapses, while the S561A mutant shows increased stability at the synapse. Moreover, we show that the S561A mutant is resistant to chemical LTP and LTD induced spine structural plasticity. Finally, we show that endogenous Ser561 phosphorylation is induced by synaptic NMDA receptor activation, and the SH3-GK domains exhibit a Ser561 phosphorylation-dependent switch to a closed conformation during chemical LTP. Taken together, we propose a model whereby synaptic NMDA receptor activation induces the phosphorylation of Ser561 in PSD-95, which promotes the SH3-GK interaction and reduces its interaction with other synaptic binding partners. This leads to increased dynamics of PSD-95 at the synapse and allows for rearrangement of the PSD. In the absence of Ser561 phosphorylation, PSD-95 is stable at the synapse, which renders the spines resistant to chemical LTP and LTD induced structural changes.

Results

Ser561 phosphorylation promotes SH3-GK interaction

Our recent studies show that Par1 phosphorylates PSD-95 on Ser561 (22). The same conserved site in Drosophila Dlg is phosphorylated by dPar1 and regulates neuromuscular junction formation (23). Ser561 is located in the GK domain of PSD-95 (Fig. 1a). The GK domain forms an intramolecular interaction with the adjacent SH3 domain, which is important for PSD-95 function (16,19). We hypothesize that Ser561 phosphorylation regulates SH3-GK interaction and thus modulates PSD-95 function. To test this hypothesis, we first performed a GST pull-down assay by incubating GST-SH3 glutathione beads with lysates from HEK293 cells expressing GFP-GK constructs. Beads were then washed and the resulting protein complex resolved by SDS-PAGE and Western blotting. Significantly less GFP-GK-S561A was pulled down with GST-SH3 as compared with wild type GFP-GK, whereas more GFP-GK-S561D was pulled down as compared with its wild type counterpart (Fig. 1b and c). This suggests that the Ser561 phosphorylation regulates the interaction between SH3 and GK domains.

To further examine this intramolecular interaction, we constructed a single chain FRET (fluorescence resonance energy transfer) biosensor (CFP-SH3-GK-YFP) (Fig.1a). Since the SH3 domain and the GK domain interact, we predict that YFP and CFP will come close enough for FRET to occur. If the SH3-GK interaction is

disrupted, it should result in lower FRET efficiency. Indeed, when the wild type probe was expressed in HEK293 cells, it showed a strong FRET signal (Fig. 1d and e). Because the very C-terminus of the GK domain forms a β-sheet that folds back to the SH3 domain (17,18), we wanted to confirm that the FRET biosensor can detect changes in intramolecular SH3-GK interactions. It has been reported that a L460P mutation in PSD-95 disrupts the intramolecular SH3-GK interaction (16). We found that the L460P mutant FRET probe exhibits significantly reduced FRET efficiency as compared with the WT probe (Fig. S1), showing that the FRET biosensor can detect changes in intramolecular SH3-GK interactions. To determine the effects of the Ser561 phosphorylation site, we expressed non-phosphorylatable and phosphomimetic mutants of the FRET probe. We found that the S561A mutant probe showed a significant decrease in FRET signal as compared with the WT probe, while the phosphomimetic S561D mutant showed an enhanced FRET signal (Fig. 1d and e). Treatment of cells with a Par1 inhibitor resulted in a significant decrease in FRET signals in the WT FRET probe (Fig. S2), suggesting that Par1-mediated phosphorylation of Ser561 is necessary for this intramolecular interaction. Overall expression levels of FRET probes were similar for all constructs (Fig. S3).

We next aimed to further confirm that the FRET signals were a result of intramolecular interactions between the SH3 and GK domains and not from intermolecular interactions. Although intramolecular SH3-GK interactions are the preferred mode of interaction, intermolecular SH3-GK interactions do occur (16). To distinguish between these two possibilities, we performed FRET spectroscopy on serial dilutions of lysates expressing different FRET constructs. At high concentrations, FRET signals can potentially come from both intra- and intermolecular interactions; however the contribution from intermolecular interactions should drop significantly with dilution. A CFP-YFP fusion protein was used as a control in which the FRET signals should primarily come from intramolecular interactions. As shown in Figure S4, FRET ratios in the CFP-YFP fusion protein gradually decreased upon dilution. FRET ratios in the WT and S561D probes decreased at similar or slower rate than the CFP-YFP fusion protein, indicating that the FRET signals in these two construct come primarily from intramolecular interactions. By contrast, FRET ratios in the S561A mutant probe rapidly decreased upon dilution, indicating that the FRET signals of the S561A mutant at high concentrations come from intermolecular interactions. This is consistent with previous studies showing that disrupting intramolecular SH3-GK interactions will facilitate intermolecular SH3-GK interactions (16).

Taken together, these results suggest that Ser561 phosphorylation promotes the intramolecular interaction between the SH3 and GK domains. When Ser561 is phosphorylated, PSD-95 shows a “closed” conformation with stronger SH3-GK interaction. If Ser561 is dephosphorylated, PSD-95 switches to an “open” conformation with weaker SH3-GK interaction.

S561A mutation of PSD-95 increases its interaction with synaptic binding partners

The GK domain binds several synaptic proteins that may influence downstream signaling cascades, including guanylate-kinase associated protein (GKAP) (24), mPins (also known as LGN) (25), and Spine-associated RapGAP (SPAR) (26,27). We examined whether Ser561 phosphorylation regulates PSD-95 interaction with these proteins, using a GST pull-down assay. We purified GST-SH3-GK constructs with or without the Ser561 mutation. For GKAP, whole brain lysates were incubated with the purified GST proteins. For SPAR and LGN, we used whole cell lysates of HEK cells expressing the respective proteins. We then analyzed bound proteins by Western blotting with antibodies targeting the above-mentioned molecules. We found that PSD-95 interaction with SPAR, GKAP and LGN were affected by Ser561 phosphorylation. The S561A mutant showed increased interaction with these proteins as compared with the wild type version (Fig. 2a-f), which was confirmed to be phosphorylated after incubation with whole cell lysates (Fig. S5) or whole brain lysates (data not shown). In addition, we found that the S561A mutant also shows increased interaction with endogenous PSD-95 (Fig. S6), which is consistent with previous reports that disrupting the intramolecular SH3-GK interaction facilitates intermolecular interactions between PSD-95

molecules (16). Taken together, these results suggest that dephosphorylation of Ser561 facilitates the interaction of the GK domain with its binding partners.

Ser561 phosphorylation regulates PSD-95 dynamics

Since Ser561 affects the interaction between PSD-95 and its synaptic binding partners, we wondered whether this would lead to altered PSD-95 dynamics at the synapse. To test this possibility, we used fluorescence recovery after photobleaching (FRAP) imaging. DIV 24 hippocampal neurons expressing different PSD-95-GFP constructs were imaged live using confocal microscopy. Single spines were photobleached using 100% laser power, and the recovery of PSD-95 fluorescence was observed over time (Fig. 3). Wild type PSD-95 recovery reached about 50% after 45 minutes. By contrast, the recovery of the S561A mutant was less than 10%, while the S561D mutant recovered to almost 80%. No significant baseline photobleaching was observed during the imaging period (Fig. S7). This suggests that Ser561 phosphorylation increases the dynamics of PSD-95 at the synapse. The increased stability of the S561A mutant at the synapse is consistent with the observed increase in the interaction of PSD-95 with multiple synaptic binding partners.

S561A mutation of PSD-95 inhibits bidirectional spine structural plasticity

Since spine plasticity involves dynamic rearrangements of the PSD scaffold, and Ser561 phosphorylation affects PSD-95 dynamics, we hypothesized that Ser561 phosphorylation regulates structural plasticity. To test this hypothesis, we used a bicistronic lentiviral vector to deplete endogenous PSD-95 and re-express a GFP-tagged PSD-95. Viral titer was controlled so that the exogenous PSD-95 was expressed at equivalent levels to the endogenous PSD-95 (Fig. 4a). Since PSD-95 overexpression blocks LTP, this strategy allows us to dissect the role of Ser561 phosphorylation without interference from the effect of PSD-95 overexpression. mRFP was then transfected into the neurons to visualize cell morphology.

To examine the effects of Ser561 phosphorylation on synaptic plasticity, we first induced chemical LTP in cultured hippocampal neurons by glycine treatment (200μM in Mg^{2+} free media, 3 min). As reported previously, glycine-induced LTP shares many features with stimulus-induced LTP that occurs in the CA1 region of the hippocampus, including activation of synaptic NMDA receptors, increased GluA1 insertion, a requirement for CaMKII activation, and dendritic spine enlargement (28-30). Consistent with previous studies (29,30), dendritic spines showed a significant enlargement in control neurons expressing a replacement wild type PSD-95-GFP. By contrast, although the PSD-95 S561A mutant did not cause any significant changes in spine size under control conditions, neurons expressing the replacement S561A mutant were resistant to glycine-induced spine enlargement (Fig. 4b-d). This suggests that Ser561 phosphorylation is important for spine enlargement during chemical LTP.

Next, we wanted to examine whether Ser561 phosphorylation is also needed for LTD. To test this possibility, we treated cultured hippocampal neurons with NMDA for 10 min, which is known to induce LTD (31). As expected, control neurons expressing a replacement wild type PSD-95-GFP showed shrinkage of dendritic spines. By contrast, neurons expressing a replacement PSD-95 S561A showed no significant changes in spine size (Fig. 4e-g), which suggests that LTD also requires Ser561 phosphorylation. Taken together, these results indicate that Ser561 phosphorylation is necessary for bidirectional spine structural plasticity.

Synaptic NMDA receptor activation induces Ser561 phosphorylation and conformational change in PSD-95

We next aimed to examine potential conformational changes in the SH3-GK domain during synaptic plasticity in live hippocampal neurons. Hippocampal neurons were transfected with the SH3-GK FRET biosensor (WT or S561A) and imaged live at DIV11. Chemical LTP was induced using glycine in Mg^{2+} free media as described above. As expected, in WT FRET biosensor expressing neurons, we observed a gradual increase in dendritic spine volume upon glycine treatment (Fig. 5a). S561A biosensor-expressing neurons did not show a signficant increase in dendritic spine volume upon glycine

induction, probably due to a dominant-negative effect of the mutant biosensor. FRET signals in the WT biosensor were significantly increased following glycine-induced chemical LTP as compared with the biosensor with the S561A mutation, suggesting that the SH3-GK domains show a Ser561 phosphorylation-dependent switch to a closed conformation during synaptic plasticity (Fig. 5a and b). The increase in FRET signals was observed throughout the spines and the dendritic shafts (Fig. 5a), likely because of the long time course of the FRET increase, the global nature of the glycine stimulation and the absence of a synaptic targeting domain in the FRET biosensor. Interestingly, although the S561A biosensor showed an overall lower FRET efficiency, both the WT and S561A biosensors exhibited an increase in FRET efficiency during the initial 25 min after glycine induction. After 25 min, the WT biosensor FRET efficiency continued to increase, while the S561A biosensor efficiency started to decrease (Fig. 5b). This suggest that there could be an additional Ser561 phosphorylation-independent transient conformational change induced by NMDA receptor activation.

Previous studies have confirmed the physiological phosphorylation of Ser561 in mammalian brains by mass spectrometry (32). However, it remains unknown whether and how this phosphorylation is regulated by synaptic activity. To examine this, we developed a phospho-specific antibody against pSer561 in PSD-95. The antibody preferentially immunoprecipitated WT PSD-95 as compared with PSD-95 S561A (Fig. S8a), and failed to immunoprecipitate PSD-95 in CIP treated samples (Fig. S8b), showing that it is specific for phosphorylated Ser561. To see whether Ser561 phosphorylation is regulated by synaptic NMDA receptor activity, we treated hippocampal neurons with picrotoxin (PTX), a $GABA_A$ receptor antagonist, and 4-aminopyridine (4-AP), a potassium channel antagonist, a combination that is known to activate synaptic NMDA receptors (33-35). Consistent with our previous studies, the MARK/Par1 kinases are stimulated by synaptic NMDA receptor activation (36) (Fig. 5c). Remarkably, Ser561 phosphorylation of PSD-95 was significantly increased by synaptic NMDA receptor activation (Fig. 5c and d), showing that endogenous phosphorylation of the Ser561 site is regulated by synaptic NMDA receptors.

Discussion

PSD-95 is perhaps one of the most extensively studied molecules at the postsynaptic density. It is well known for its involvement in synaptic maturation and plasticity. Yet despite numerous studies showing a role for PSD-95 in synaptic plasticity, there is still a lack of detailed mechanistic insight into how PSD-95 is regulated both structurally and functionally during activity-dependent plasticity. Since PSD-95 is a scaffolding protein that lacks any enzymatic activity, one of the likely modes of regulation is through posttranslational modifications that change protein-protein interactions and possibly cause conformational changes in PSD-95. While several phosphorylation sites have been identified in PSD-95 (37-42), how these sites regulate PSD-95 structure and function during plasticity is still not well understood.

In this study, we show that Ser561 phosphorylation of PSD-95 regulates its dynamics and conformation and is important for bidirectional spine structural plasticity. We show that Ser561 regulates the intramolecular interaction between the SH3 and GK domains of PSD-95. Pull-down experiments and FRET imaging show that Ser561 phosphorylation promotes the interaction between SH3 and GK domains, leading to a “closed” conformation of PSD-95, while the non-phosphorylatable S561A mutant shows decreased SH3-GK interaction and an “open” conformation. We further show that the S561A mutant exhibit increased binding to proteins that normally interact with the GK domain, including GKAP, SPAR, and LGN/mPins. These data suggest that dephosphorylation of Ser561 facilitates protein-protein interactions between the GK domain of PSD-95 and its interacting partners.

In addition, we show that Ser561 phosphorylation regulates PSD-95 dynamics. Using FRAP imaging, we show that compared with wild type PSD-95, the S561A mutant is more stably incorporated at the synapse, while the phosphomimetic S561D mutant is more dynamic. This is consistent with our data showing that the S561A mutant exhibits increased interaction with its synaptic binding partners. Moreover, using

chemical LTP and LTD protocols, we show that the S561A mutant is resistant to chemical LTP or LTD-induced changes in spine size, suggesting that Ser561 phosphorylation is necessary for spine structural plasticity. Finally, we show that endogenous Ser561 phosphorylation is induced by synaptic NMDA receptor activation, and the SH3-GK domains exhibit a Ser561 phosphorylation-dependent switch to a closed conformation during glycine-induced LTP. Taken together, these data indicate that Ser561 phosphorylation is important for bidirectional dendritic spine structural plasticity. Because of the global nature of the chemical LTP and LTD induction methods, it would be of interest to determine the role of the Ser561 phosphorylation of PSD-95 during plasticity at the single spine level.

What might be the underlying mechanism by which Ser561 phosphorylation regulates PSD-95 protein-protein interaction and conformation? Interestingly, Ser561 is not one of the few residues known to be required for SH3-GK intramolecular binding (17). It is, however, within the GMP-binding site of the GK domain known to mediate the interactions with proteins like GKAP, LGN and MAP1A (43,44). It is likely that phosphorylation of Ser561 will block the GMP-binding site, causing weakened interactions between PSD-95 and its GK domain interacting partners. Further, we speculate that the Ser561 phosphorylation may allosterically alter SH3-GK interactions leading to conformational changes in PSD-95. Consistent with our hypothesis, previous studies have shown allosteric control of SH3-GK interactions that involves residues distant from the SH3-GK binding interface (45).

Taken together, our data show a novel role for NMDA receptor-dependent Ser561 phosphorylation of PSD-95 in regulating its dynamics and conformation and promoting dendritic spine plasticity. Together with our recent data showing that MARK/Par1 is activated downstream of NMDA receptors through a PKA-dependent mechanism (36), we propose the following model (Fig. 5e). When Ser561 of PSD-95 is de-phosphorylated, the SH3-GK domains show an open conformation. In addition, de-phosphorylation of Ser561 facilitates interaction between PSD-95 and its GK domain binding partners, which makes PSD-95 stably incorporated at the synapse. Upon plasticity-inducing stimuli, NMDA receptors are activated, which leads to the downstream activation of MARK/Par1 and the phosphorylation of Ser561 in PSD-95. Ser561 phosphorylation leads to an increase in SH3-GK interaction and switches PSD-95 to the "closed" conformation. Further, it reduces PSD-95 interaction with its binding partners and increases PSD-95 dynamics. This allows PSD-95 to temporarily leave the PSD scaffold, which permits dynamic rearrangement of the PSD. Our data are consistent with the observation that PSD-95 temporarily leaves the PSD during synaptic plasticity (37). Together, our studies provide novel, mechanistic insight into the regulation of PSD-95 during dendritic spine structural plasticity and may shed light on the regulation of other MAGUK family proteins, since the serine site is conserved across multiple members of the MAGUK family (23).

Experimental Procedures

DNA constructs

GW1-PSD-95-GFP construct was a generous gift from Dr. Ann Marie Craig (University of British Columbia). The S561A and S561D mutants of PSD-95 were generated by site-directed mutagenesis using GW1-PSD-95-GFP as the template. For construction of GST and GFP fusion proteins of PSD-95 fragments, the domains (SH3, aa 412–509; GK, aa 510–724; SH3-GK, aa 412–724) were PCR amplified using rat PSD-95 in GW1 as the template and subcloned into EcoRI-NotI sites (SH3, SH3-GK) in pGEX-4T-1 vector or NotI-EcoRI sites (GK) in pKvenus vector. For construction of single chain FRET probe, the domains (SH3-GK, aa 412–724) were PCR amplified using rat PSD-95 in GW1 as the template and subcloned into BamHI-EcoRI sites of pKseFRET vector (46). For simultaneous knockdown of endogenous PSD-95 and re-expressing the PSD-95-GFP mutants, PSD-95 shRNA (14) was cloned into the pLVTHM vector after the H1 RNA promoter. PSD-95 constructs with silent mutations that make them resistant to the shRNA were cloned into the same vector after the EF1α promoter. pLV-venus-LGN construct was a generous gift from Drs. Yongliang Huo and Ian G. Macara (Vanderbilt University). Myc-SPAR construct was a generous gift from Dr. Daniel Pak (Georgetown University).

Neuronal culture, transfections and treatments
Hippocampal neuron cultures were prepared from embryonic rats as described previously (22,47-49). Cultures were grown in Neurobasal medium (Invitrogen) supplemented with B-27 (Invitrogen) and 2 mM GlutaMAX (Invitrogen). Neurons were transfected using Effectene transfection reagent (Qiagen). For FRAP imaging, neurons were transfected at 13 days in vitro (DIV) and imaged at DIV24.

For chemical LTP (cLTP) and chemical LTD (cLTD), hippocampal neurons were infected at 0 DIV by lentivirus expressing the bicistronic PSD-95 constructs, and transfected at 13 DIV with mRFP to visualize spines. For cLTP, hippocampal neurons were treated with glycine (Sigma-Aldrich; 200 μM) in Mg^{2+}-free Hank's Balanced Salt Solution (HBSS, Sigma-Aldrich) containing 2 mM $CaCl_2$ for 3 min on DIV17 and then transferred to HBSS with Ca^{2+} but without any added glycine for 60 min. For cLTD, hippocampal neurons on the coverslips were treated with N-methyl-D-aspartic acid (NMDA) (Sigma-Aldrich; 50 μM) in Mg^{2+}-free HBSS containing 1.8 mM $CaCl_2$ and 1 μM glycine for 10 min on DIV21 and then transferred to the same solution without any added NMDA for 60 min. Neurons were then fixed in 4% paraformaldehyde with 4% sucrose in PBS for 15 min at room temperature. For synaptic NMDA receptor stimulation, neurons were treated with 4-AP(Sigma, 1mM final) and picrotoxin (Sigma, 10μM final) for 10 min and lysed as described previously (36). Par1/MARK inhibitor (MRT00207148) was a generous gift from Dr. Janet Brownlees (Medical Research Council Technology, London, UK) and was used at 10μM final concentration.

GST pull-down assay, immunoprecipitation and Western Blotting
For GST pull-down assay and co-immunoprecipitation, HEK293 cells expressing different plasmid constructs or whole brain tissue were lysed on ice in buffer containing 25 mM Hepes, 150 mM NaCl, 10 mM $MgCl_2$, 1% Nonidet P-40, and 10 mM DTT and supplemented with protease inhibitor cocktail (Sigma-Aldrich), phosphatase inhibitor cocktail (Sigma-Aldrich), 10 mM β-glycerophosphate, and 10 mM NaF. Lysates were cleared by centrifugation at 13,000×g for 10 min at 4°C. GST fusion proteins were purified using glutathione-Sepharose beads (GE Healthcare) according to manufacturer's instructions. Beads with bound GST proteins were incubated with lysates from HEK cells or whole brain lysates for 3 hours at 4°C. For co-immunoprecipitation, cell lysates were incubated with anti-GFP antibody (2 μg, Invitrogen A11122) for 1 h at 4 °C, followed by incubation with 20 μl of Dynabeads Protein G, which was preblocked with 5% BSA in lysis buffer. Beads were washed three times with lysis buffer. Bound proteins were eluted with 3×sample buffer and subjected to SDS-PAGE and Western blot analysis.

For detecting endogenous phosphorylation of the Ser561 site, we developed a rabbit polyclonal phospho-specific antibody against pSer561 of PSD-95 (AbMart) using the phospho-peptide PDKFGpSCVPHT. pSer561 antibody (10 μg) was used for immunoprecipitation from hippocampal lysates as described above, and the immunoprecipitate was analyzed by Western blotting with PSD-95 antibody. For the CIP control, lysates of HEK293 cells expressing PSD-95 constructs were treated with calf intestinal alkaline phosphatase (CIP) for 1 hour at 37°C before immunoprecipitation with the pSer561 antibody.

For Western blot analysis, the primary antibodies used were rabbit anti-Myc antibody (1:2,000; A-14, Santa Cruz Biotechnology, Santa Cruz, CA), rabbit anti-GFP antibody (1:4,000; a generous gift from Dr. Ian Macara), mouse anti-GKAP antibody (1:500, NeuroMab, Davis, CA), rabbit anti-phosphoserine antibody (1:1000, Abcam, Cambridge, MA), mouse anti-PSD-95 antibody (1:1,000, 6G6, Santa Cruz Biotechnology, Santa Cruz, CA; K28/43, NeuroMab, UC Davis), phospho-MARK family (Thermo Scientific, Cat. No. PA5-17495, 1:1000), and MARK1/Par1c (ProteinTech, Cat. No. 21552-1-AP, 1:1000). Horseradish peroxidase-conjugated goat anti-rabbit and anti-mouse antibodies (Jackson ImmunoResearch Laboratories, West Grove, PA) were used at 1:3,000 dilution. Proteins were visualized by enhanced chemiluminescence and imaged using a Syngene G:BOX iChemi XR system and GeneSnap software (Version 7.09.a;

Syngene USA, Frederick, MD), or an Amersham Imager 600 (GE Healthcare).

Fluorescence resonance energy transfer (FRET) imaging and spectroscopy

FRET imaging was performed on an Olympus FV1000 confocal microscope with a LUMPLFLN 60× water immersion lens (NA 1.00). The 405 nm laser was used with a 405/440 dichroic mirror to excite CFP. CFP emission was collected in one channel spanning 480–495 nm and YFP emission was collected in 535-565nm. Live cell FRET images were acquired using the sensitized emission module in Olympus Fluoview software. FRET efficiency images were generated using the sensitized emission module of Olympus Fluoview software after background subtraction, correction for donor and acceptor bleedthrough and for expression levels of the biosensor. For FRET efficiency measurements in live cells, images of each channel were acquired before and after photobleaching of YFP. The following formula was used to calculate the FRET efficiency of each construct:

$$FRET\ efficiency = 1 - \frac{Prebleaching}{Postbleaching}$$

For time-lapse FRET imaging in live neurons, ratio imaging of the FRET channel over the CFP channel was performed to visualize FRET efficiency changes over time using the ratio imaging module in the Olympus Fluoview software. FRET/CFP ratios in dendritic spines were quantified and normalized to the FRET/CFP ratio at the 0 min time point.

For FRET spectroscopy, HEK293 cells expressing different FRET constructs were lysed. Emission spectra of the lysates between 450 nm and 550 nm were measured with 430 nm excitation using a Biotek Synergy H1 multi-mode plate reader.

Fluorescence recovery after photobleaching (FRAP)

FRAP experiments was performed at 37°C with an Olympus FV1000 confocal microscope with a LUMPLFLN 60× water immersion lens (NA 1.00). Hippocampal neurons were transfected with GFP-tagged PSD-95 constructs. PSD-95 clusters at the spine head were bleached using 488 nm laser set at 100% laser power. Time lapse images were collected before and after photobleaching using 5% laser power, and the fluorescent intensities of the bleached spot were quantified using ImageJ and plotted as a function of time.

Image quantification

Dendritic spine morphology was quantified by two individuals who were blind to the experimental conditions, and the results were averaged. Dendritic spines were defined as stubby or mushroom-shaped protrusions and contacted by presynaptic terminals. Spine length and width were measured using ImageJ. Spine length was defined as the length from the tip of the spine head to the point where the spine joins the dendrite. Spine width was defined as the maximal width of the spine head perpendicular to the long axis of the spine neck. 1500-1800 spines from at least 15 neurons for cLTP and 1200-1600 spines from at least 15 neurons for cLTD were measured.

Statistical analysis

Statistical analysis was performed using GraphPad Prism. For all Western blot data, scatter plots are shown with mean ± SD. The number of independent biological replicates are indicated in the figure legends. Quantification of imaging data are shown as either mean ± SD, or box-whisker plots. Box denotes 25th and 75th percentiles, line within box denotes median and whiskers denote min and max values. Number of neurons/dendritic spines quantified are indicated in the figure legends. Data were analyzed by one-way or two-way ANOVA with Tukey's *post hoc* test for multiple group comparisons. Student's t-test was used for comparison between two groups. One sample t-test was used for Western blot data in which the control levels are normalized to one. $P<0.05$ is considered statistically significant.

Acknowledgements

We would like to thank Drs. Ann Marie Craig (University of British Columbia), Daniel Pak (Georgetown University), Janet Brownlees (Medical Research Council Technology, London, UK), Ian Macara and

Yongliang Huo (Vanderbilt University) for reagents. We would also like to thank Anna Damato and Merry Zhai for assistance with data analysis, and Drs. Mladen-Roko Rasin, Michael Matise, Terri Kinzy and Peter Lobel for access to their equipment. This work was supported by NIH grants NS065183, NS089578 and startup funds from the Rutgers Robert Wood Johnson Medical School to HZ.

Conflict of Interest

The authors declare that they have no conflict of interest.

Author Contributions

QW and HZ designed the study. QW, MS and LPB performed the experiments. QW, MS and HZ analyzed the data. QW and HZ wrote the manuscript. All authors reviewed the results and approved the final version of the manuscript.

References

1. Lai, C. S., Franke, T. F., and Gan, W. B. (2012) Opposite effects of fear conditioning and extinction on dendritic spine remodelling. *Nature* **483**, 87-91
2. Yang, G., Pan, F., and Gan, W. B. (2009) Stably maintained dendritic spines are associated with lifelong memories. *Nature* **462**, 920-924
3. Fu, M., Yu, X., Lu, J., and Zuo, Y. (2012) Repetitive motor learning induces coordinated formation of clustered dendritic spines in vivo. *Nature* **483**, 92-95
4. Xu, T., Yu, X., Perlik, A. J., Tobin, W. F., Zweig, J. A., Tennant, K., Jones, T., and Zuo, Y. (2009) Rapid formation and selective stabilization of synapses for enduring motor memories. *Nature* **462**, 915-919
5. Yu, X., and Zuo, Y. (2011) Spine plasticity in the motor cortex. *Curr Opin Neurobiol* **21**, 169-174
6. Colgan, L. A., and Yasuda, R. (2013) Plasticity of Dendritic Spines: Subcompartmentalization of Signaling. *Annu Rev Physiol*
7. Bosch, M., and Hayashi, Y. (2012) Structural plasticity of dendritic spines. *Curr Opin Neurobiol* **22**, 383-388
8. Anggono, V., and Huganir, R. L. (2012) Regulation of AMPA receptor trafficking and synaptic plasticity. *Curr Opin Neurobiol* **22**, 461-469
9. Nagerl, U. V., Eberhorn, N., Cambridge, S. B., and Bonhoeffer, T. (2004) Bidirectional activity-dependent morphological plasticity in hippocampal neurons. *Neuron* **44**, 759-767
10. Zhou, Q., Homma, K. J., and Poo, M. M. (2004) Shrinkage of dendritic spines associated with long-term depression of hippocampal synapses. *Neuron* **44**, 749-757
11. Okamoto, K., Nagai, T., Miyawaki, A., and Hayashi, Y. (2004) Rapid and persistent modulation of actin dynamics regulates postsynaptic reorganization underlying bidirectional plasticity. *Nat Neurosci* **7**, 1104-1112
12. Xu, W. (2011) PSD-95-like membrane associated guanylate kinases (PSD-MAGUKs) and synaptic plasticity. *Curr Opin Neurobiol* **21**, 306-312
13. Stein, V., House, D. R., Bredt, D. S., and Nicoll, R. A. (2003) Postsynaptic density-95 mimics and occludes hippocampal long-term potentiation and enhances long-term depression. *J Neurosci* **23**, 5503-5506
14. Xu, W., Schluter, O. M., Steiner, P., Czervionke, B. L., Sabatini, B., and Malenka, R. C. (2008) Molecular dissociation of the role of PSD-95 in regulating synaptic strength and LTD. *Neuron* **57**, 248-262
15. Ehrlich, I., Klein, M., Rumpel, S., and Malinow, R. (2007) PSD-95 is required for activity-driven synapse stabilization. *Proc Natl Acad Sci U S A* **104**, 4176-4181
16. McGee, A. W., and Bredt, D. S. (1999) Identification of an intramolecular interaction between the SH3 and guanylate kinase domains of PSD-95. *J Biol Chem* **274**, 17431-17436
17. Tavares, G. A., Panepucci, E. H., and Brunger, A. T. (2001) Structural characterization of the intramolecular interaction between the SH3 and guanylate kinase domains of PSD-95. *Mol Cell* **8**, 1313-1325
18. McGee, A. W., Dakoji, S. R., Olsen, O., Bredt, D. S., Lim, W. A., and Prehoda, K. E. (2001) Structure of the SH3-guanylate kinase module from PSD-95 suggests a mechanism for regulated assembly of MAGUK scaffolding proteins. *Mol Cell* **8**, 1291-1301
19. Shin, H., Hsueh, Y. P., Yang, F. C., Kim, E., and Sheng, M. (2000) An intramolecular interaction between Src homology 3 domain and guanylate kinase-like domain required for channel clustering by postsynaptic density-95/SAP90. *J Neurosci* **20**, 3580-3587
20. Bhattacharyya, S., Biou, V., Xu, W., Schluter, O., and Malenka, R. C. (2009) A critical role for PSD-95/AKAP interactions in endocytosis of synaptic AMPA receptors. *Nat Neurosci* **12**, 172-181

21. Woods, D. F., Hough, C., Peel, D., Callaini, G., and Bryant, P. J. (1996) Dlg protein is required for junction structure, cell polarity, and proliferation control in Drosophila epithelia. *J Cell Biol* **134**, 1469-1482
22. Wu, Q., DiBona, V. L., Bernard, L. P., and Zhang, H. (2012) The polarity protein partitioning-defective 1 (PAR-1) regulates dendritic spine morphogenesis through phosphorylating postsynaptic density protein 95 (PSD-95). *J Biol Chem* **287**, 30781-30788
23. Zhang, Y., Guo, H., Kwan, H., Wang, J. W., Kosek, J., and Lu, B. (2007) PAR-1 kinase phosphorylates Dlg and regulates its postsynaptic targeting at the Drosophila neuromuscular junction. *Neuron* **53**, 201-215
24. Kim, E., Naisbitt, S., Hsueh, Y. P., Rao, A., Rothschild, A., Craig, A. M., and Sheng, M. (1997) GKAP, a novel synaptic protein that interacts with the guanylate kinase-like domain of the PSD-95/SAP90 family of channel clustering molecules. *J Cell Biol* **136**, 669-678
25. Sans, N., Wang, P. Y., Du, Q., Petralia, R. S., Wang, Y. X., Nakka, S., Blumer, J. B., Macara, I. G., and Wenthold, R. J. (2005) mPins modulates PSD-95 and SAP102 trafficking and influences NMDA receptor surface expression. *Nat Cell Biol* **7**, 1179-1190
26. Kim, E., and Sheng, M. (2004) PDZ domain proteins of synapses. *Nat Rev Neurosci* **5**, 771-781
27. Pak, D. T., Yang, S., Rudolph-Correia, S., Kim, E., and Sheng, M. (2001) Regulation of dendritic spine morphology by SPAR, a PSD-95-associated RapGAP. *Neuron* **31**, 289-303
28. Lu, W., Man, H., Ju, W., Trimble, W. S., MacDonald, J. F., and Wang, Y. T. (2001) Activation of synaptic NMDA receptors induces membrane insertion of new AMPA receptors and LTP in cultured hippocampal neurons. *Neuron* **29**, 243-254
29. Fortin, D. A., Davare, M. A., Srivastava, T., Brady, J. D., Nygaard, S., Derkach, V. A., and Soderling, T. R. (2010) Long-term potentiation-dependent spine enlargement requires synaptic Ca2+-permeable AMPA receptors recruited by CaM-kinase I. *J Neurosci* **30**, 11565-11575
30. Park, M., Salgado, J. M., Ostroff, L., Helton, T. D., Robinson, C. G., Harris, K. M., and Ehlers, M. D. (2006) Plasticity-induced growth of dendritic spines by exocytic trafficking from recycling endosomes. *Neuron* **52**, 817-830
31. Pontrello, C. G., Sun, M. Y., Lin, A., Fiacco, T. A., DeFea, K. A., and Ethell, I. M. (2012) Cofilin under control of beta-arrestin-2 in NMDA-dependent dendritic spine plasticity, long-term depression (LTD), and learning. *Proc Natl Acad Sci U S A* **109**, E442-451
32. Trinidad, J. C., Barkan, D. T., Gulledge, B. F., Thalhammer, A., Sali, A., Schoepfer, R., and Burlingame, A. L. (2012) Global identification and characterization of both O-GlcNAcylation and phosphorylation at the murine synapse. *Mol Cell Proteomics* **11**, 215-229
33. Hoey, S. E., Williams, R. J., and Perkinton, M. S. (2009) Synaptic NMDA receptor activation stimulates alpha-secretase amyloid precursor protein processing and inhibits amyloid-beta production. *J Neurosci* **29**, 4442-4460
34. Hou, H., Sun, L., Siddoway, B. A., Petralia, R. S., Yang, H., Gu, H., Nairn, A. C., and Xia, H. (2013) Synaptic NMDA receptor stimulation activates PP1 by inhibiting its phosphorylation by Cdk5. *J Cell Biol* **203**, 521-535
35. Hardingham, G. E., Fukunaga, Y., and Bading, H. (2002) Extrasynaptic NMDARs oppose synaptic NMDARs by triggering CREB shut-off and cell death pathways. *Nat Neurosci* **5**, 405-414
36. Bernard, L. P., and Zhang, H. (2015) MARK/Par1 Kinase Is Activated Downstream of NMDA Receptors through a PKA-Dependent Mechanism. *PLoS One* **10**, e0124816
37. Steiner, P., Higley, M. J., Xu, W., Czervionke, B. L., Malenka, R. C., and Sabatini, B. L. (2008) Destabilization of the postsynaptic density by PSD-95 serine 73 phosphorylation inhibits spine growth and synaptic plasticity. *Neuron* **60**, 788-802
38. Nelson, C. D., Kim, M. J., Hsin, H., Chen, Y., and Sheng, M. (2013) Phosphorylation of threonine-19 of PSD-95 by GSK-3beta is required for PSD-95 mobilization and long-term depression. *J Neurosci* **33**, 12122-12135

39. Kim, M. J., Futai, K., Jo, J., Hayashi, Y., Cho, K., and Sheng, M. (2007) Synaptic accumulation of PSD-95 and synaptic function regulated by phosphorylation of serine-295 of PSD-95. *Neuron* **56**, 488-502
40. Zhang, J., Lewis, S. M., Kuhlman, B., and Lee, A. L. (2013) Supertertiary structure of the MAGUK core from PSD-95. *Structure* **21**, 402-413
41. Zhang, J., Petit, C. M., King, D. S., and Lee, A. L. (2011) Phosphorylation of a PDZ domain extension modulates binding affinity and interdomain interactions in postsynaptic density-95 (PSD-95) protein, a membrane-associated guanylate kinase (MAGUK). *J Biol Chem* **286**, 41776-41785
42. Ballif, B. A., Carey, G. R., Sunyaev, S. R., and Gygi, S. P. (2008) Large-scale identification and evolution indexing of tyrosine phosphorylation sites from murine brain. *J Proteome Res* **7**, 311-318
43. Reese, M. L., Dakoji, S., Bredt, D. S., and Dotsch, V. (2007) The guanylate kinase domain of the MAGUK PSD-95 binds dynamically to a conserved motif in MAP1a. *Nat Struct Mol Biol* **14**, 155-163
44. Zhu, J., Shang, Y., Xia, C., Wang, W., Wen, W., and Zhang, M. (2011) Guanylate kinase domains of the MAGUK family scaffold proteins as specific phospho-protein-binding modules. *EMBO J* **30**, 4986-4997
45. Marcette, J., Hood, I. V., Johnston, C. A., Doe, C. Q., and Prehoda, K. E. (2009) Allosteric control of regulated scaffolding in membrane-associated guanylate kinases. *Biochemistry* **48**, 10014-10019
46. Hao, Y., and Macara, I. G. (2008) Regulation of chromatin binding by a conformational switch in the tail of the Ran exchange factor RCC1. *J Cell Biol* **182**, 827-836
47. Zhang, H., and Macara, I. G. (2006) The polarity protein PAR-3 and TIAM1 cooperate in dendritic spine morphogenesis. *Nat Cell Biol* **8**, 227-237
48. Zhang, H., and Macara, I. G. (2008) The PAR-6 polarity protein regulates dendritic spine morphogenesis through p190 RhoGAP and the Rho GTPase. *Dev Cell* **14**, 216-226
49. Sun, M., Bernard, L. P., Dibona, V. L., Wu, Q., and Zhang, H. (2013) Calcium phosphate transfection of primary hippocampal neurons. *J Vis Exp*, e50808

Figure Legends

Figure 1. Effects of Ser561 phosphorylation mutants of PSD-95 on SH3-GK interaction.

a. A schematic representation of the structure of PSD-95 and the single chain FRET probes (CFP-SH3-GK-YFP with or without mutation).
b. GST pull-down assay. HEK293 cells expressing GFP-GK or GFP-GK-S561A/D were incubated with GST-SH3 beads. GST beads were used as a control. The bound proteins were analyzed by Western blotting (WB) with a GFP antibody.
c. Quantification for GST pull-down assay revealed significantly less GFP-GK-S561A was pulled down with GST-SH3 as compared with wild type GFP-GK, whereas more GFP-GK-S561D was pulled down as compared with the wild type counterpart. Data are shown as scatter plot with mean±SD, n=3 independent experiments, *p<0.05, **p<0.01, ***p<0.001 by one-way ANOVA with Tukey's *post hoc* test.
d. Representative FRET images of the CFP-SH3-GK-YFP and mutants in HEK293 cells. CFP-YFP fusion was used as a positive control, and co-transfected CFP and YFP were used as a negative control. FRET efficiency images were generated using the sensitized emission module of Olympus Fluoview after background subtraction, correction for donor and acceptor bleedthrough and for expression levels of the biosensor. Scale bar: 10 μm.
e. Quantification of FRET efficiency using the acceptor photobleaching method. Significantly decreased FRET efficiency in the FRET construct with S561A mutation, and significantly increased FRET efficiency in the S561D mutant were observed. Box denotes 25th and 75th percentiles, line within box denotes median and whiskers denote min and max values. 50 cells per group from three independent experiments were analyzed. **** p<0.0001 by one-way ANOVA with Tukey's *post hoc* test.

Figure 2. S561A mutation facilitates the interaction between PSD-95 and its synaptic binding partners.

a. GST pull-down assay for GKAP. GST or GST-SH3-GK WT /S561A beads were incubated with whole brain lysates. Bound proteins were analyzed by Western blotting with the GKAP antibody.
b. Quantification of blots in (a) shown as scatter plot with mean ± SD, n=4, *p<0.05 by one sample t-test.
c. GST pull-down assay for LGN. GST or GST-SH3-GK WT /S561A beads were incubated with lysates from HEK293 cells expressing venus-LGN. Bound proteins were analyzed by Western blotting with GFP antibody.
d. Quantification of blots in (c) shown as scatter plot with mean ± SD, n=5, ***p<0.001 by one sample t-test.
e. GST pull-down assay for SPAR. GST or GST-SH3-GK WT/S561A beads were incubated with lysates from HEK293 cells expressing myc-SPAR. Bound proteins were analyzed by Western blotting with myc antibody.
f. Quantification of blots in (e) shown as scatter plot with mean ± SD, n=7, **p<0.01 by one sample t-test.

Figure 3. Effects of Ser561 phosphorylation mutants on PSD-95 dynamics at the synapse.

a. Representative time-lapse FRAP images of PSD-95-GFP constructs in DIV 24 hippocampal neurons. PSD-95 clusters at the spine head (yellow arrow) were bleached using 488 nm laser set at 100% laser power and the fluorescence recovery was followed over time. Scale bar: 2 μm.
b. Data were quantified and shown as mean ± SD, n=30-35 spines from 16 hippocampal neurons per group. **p<0.0001 by two-way ANOVA with Tukey's *post doc* test.

Figure 4. PSD-95 S561A mutant inhibits bidirectional spine structural plasticity.

a. Cortical neurons were infected with lentivirus expressing a bicistronic vector that simultaneously knocks down endogenous PSD-95 and re-expresses a GFP-tagged PSD-95 construct. Neurons were lysed and subjected to Western blot analysis.
b. Hippocampal neurons were infected by the bicistronic lentivirus at DIV0 and transfected with mRFP at DIV13 to visualize cell morphology. At DIV17, neurons were stimulated by 200 μM glycine in Mg^{2+} free media for 3 min to induce chemical LTP. Representative images of secondary dendrites are shown. Scale bar is 2 μm.
c. Quantification of spine length and width for b. Data are shown as cumulative curves. 'ctrl'=control treatment with the same Mg^{2+} free media without glycine. 'Gly'=Glycine treatment.
d. Quantifications of spine length and width for b. Data are shown as box and whisker plots, n = 1500-1800 spines from at least 15 neurons. ****p<0.0001 by two-way ANOVA with Tukey's *post doc* test.
e. Hippocampal neurons were infected by the bicistronic lentivirus at DIV0 and transfected with mRFP at DIV13 to visualize cell morphology. At DIV21, neurons were stimulated by 50 μM NMDA for 10 min to induce chemical LTD. Representative images of secondary dendrites are shown. Scale bar is 2 μm.
f. Quantification of spine length and width for a. Data are shown as cumulative curves. 'ctrl'=control treatment with the same media without NMDA. 'NMDA'=NMDA treatment.
g. Quantifications of spine length and width. Data are shown as box and whisker plots, n = 1200-1600 spines from at least 15 neurons. ****p<0.0001 by two-way ANOVA with Tukey's *post hoc* test.

Figure 5. Synaptic NMDA receptor activation induces Ser561 phosphorylation and conformational change in PSD-95.

a. Hippocampal neurons were transfected with the CFP-SH3-GK-YFP (WT or S561A) biosensors and imaged live at DIV11. Neurons were treated with 200μM glycine in Mg^{2+} free media for 3 min and time lapse images of the CFP channel and the FRET channel were collected before and after stimulation. FRET/CFP ratio images were acquired using the Olympus Fluoview ratio imaging module. Contours of the dendrites were delineated by white lines. Scale bar: 5 μm.
b. Quantification of FRET/CFP ratio over time in dendritic spines in the WT and S561A FRET biosensors. Data are mean ± SD, *p<0.05, ***p<0.001 by Student's t-test, n=1000-1500 spines from 8-13 neurons.
c. Hippocampal neurons (DIV11) were treated with 1mM 4-AP and 10 μM picrotoxin (PTX) for 10 min, lysed and immunoprecipitated with the pSer561 antibody. Immunoprecipitates were blotted for PSD-95 and inputs were blotted for PSD-95, p-Par1 and Par1.
d. Quantification of the pSer561 levels in c, normalized to control. ***p<0.01 by one sample t-test, n=8.
e. Working model. PSD-95 without Ser561 phosphorylation has an open conformation and stronger interactions with other synaptic binding partners, which renders it stably incorporated at the PSD. Upon plasticity-inducing stimuli, NMDA receptors are activated, which leads to downstream activation of MARK/Par1 and the phosphorylation of PSD-95 at Ser561. This leads to a

conformational change in the SH3-GK domain of PSD-95 and decreases the interaction of PSD-95 with synaptic binding partners, which allows PSD-95 to temporarily leave the PSD. This temporary dissociation of PSD-95 is necessary for the dynamic rearrangement of the PSD scaffold during bidirectional spine structural plasticity.

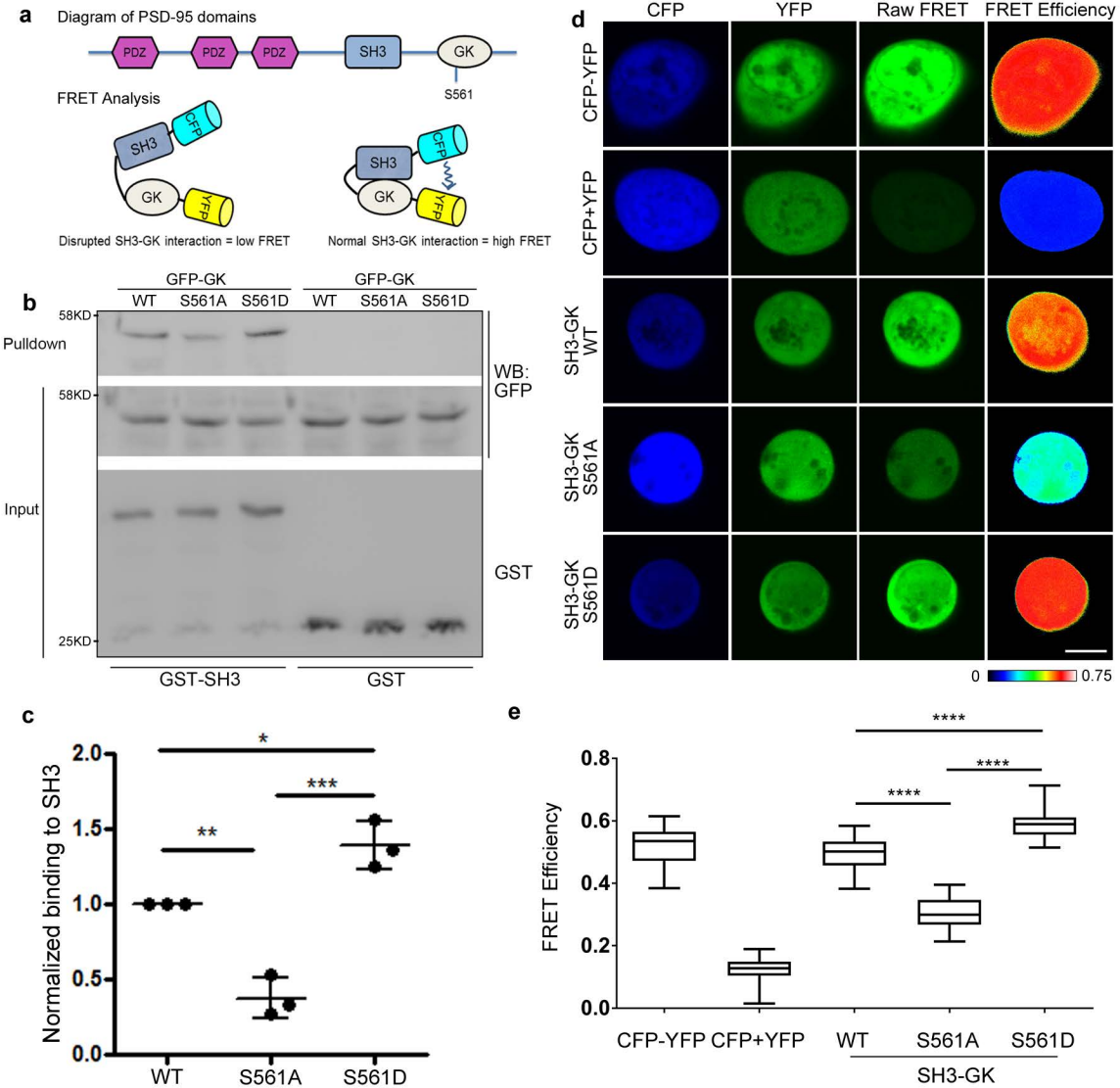
a
Diagram of PSD-95 domains
PDZ
PDZ
PDZ
SH3
GK
S561
FRET Analysis
SH3
CFP
GK
YFP
Disrupted SH3-GK interaction = low FRET
Normal SH3-GK interaction = high FRET
b
GFP-GK
WT
S561A
S561D
GFP-GK
WT
S561A
S561D
58KD
Pulldown
58KD
WB: GFP
Input
GST
25KD
GST-SH3
GST
c
Normalized binding to SH3
2.0
1.5
1.0
0.5
0.0
*
**
***
WT
S561A
S561D
d
CFP
YFP
Raw FRET
FRET Efficiency
CFP-YFP
CFP+YFP
SH3-GK WT
SH3-GK S561A
SH3-GK S561D
0
0.75
e
FRET Efficiency
0.8
0.6
0.4
0.2
0.0
****
****
****
CFP-YFP
CFP+YFP
WT
S561A
S561D
SH3-GK

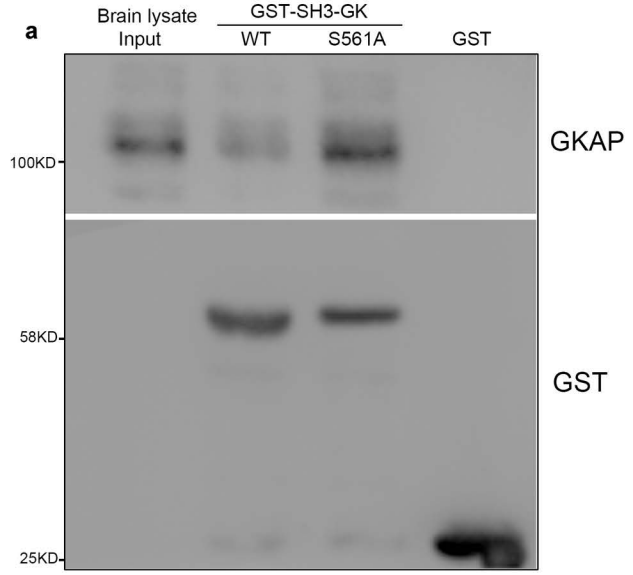
a
Brain lysate Input
GST-SH3-GK
WT
S561A
GST
GKAP
GST
100KD
58KD
25KD

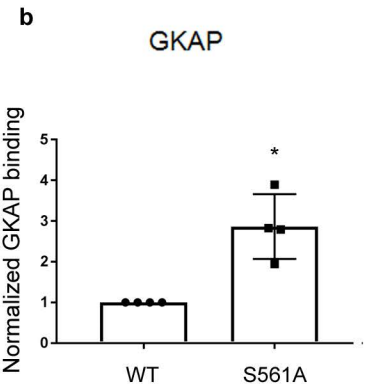
b
GKAP
Normalized GKAP binding
*
WT
S561A

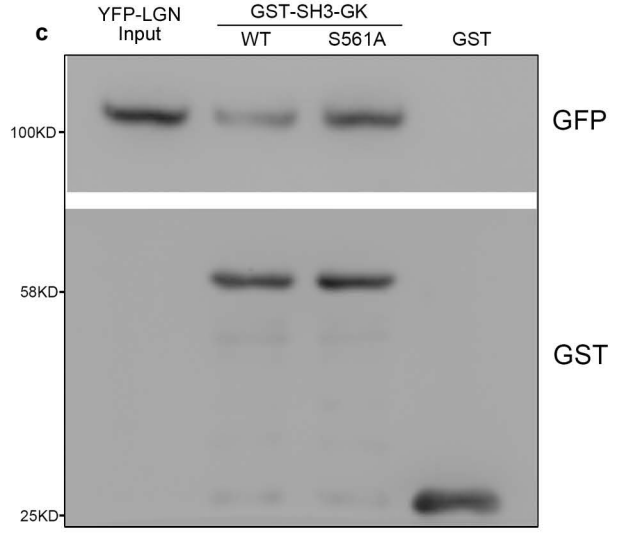
c
YFP-LGN Input
GST-SH3-GK
WT
S561A
GST
GFP
GST
100KD
58KD
25KD

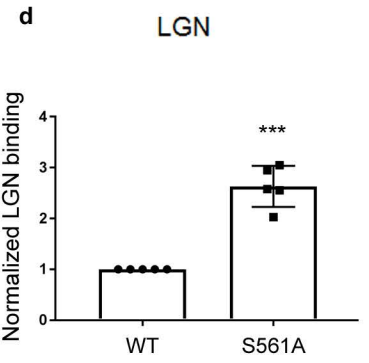
d
LGN
Normalized LGN binding
***
WT
S561A

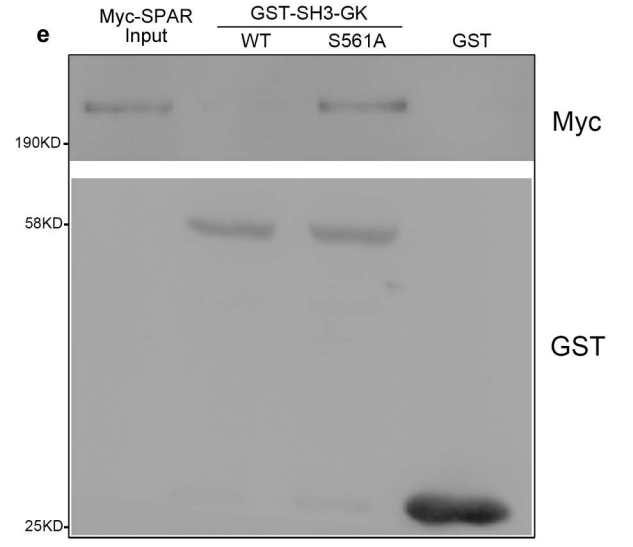
e
Myc-SPAR Input
GST-SH3-GK
WT
S561A
GST
Myc
GST
190KD
58KD
25KD

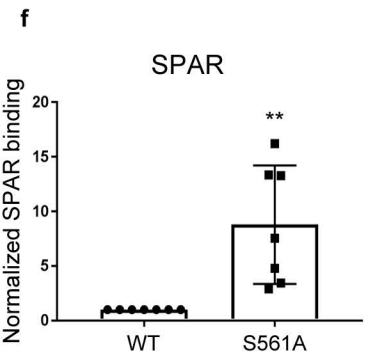
f
SPAR
Normalized SPAR binding
**
WT
S561A

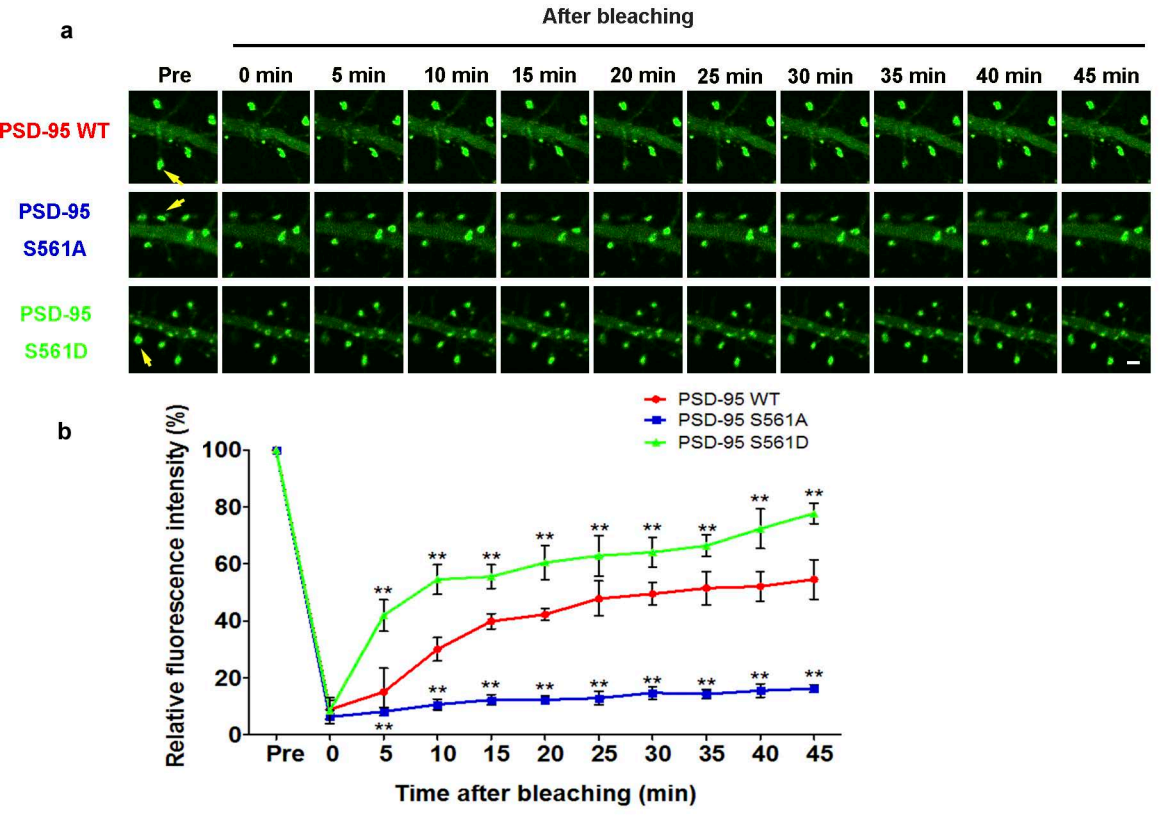
a
After bleaching
Pre
0 min
5 min
10 min
15 min
20 min
25 min
30 min
35 min
40 min
45 min
PSD-95 WT
PSD-95
S561A
PSD-95
S561D
b
PSD-95 WT
PSD-95 S561A
PSD-95 S561D
Relative fluorescence intensity (%)
100
80
60
40
20
0
Pre
0
5
10
15
20
25
30
35
40
45
Time after bleaching (min)
**

Wu and Sun et al. Figure 4

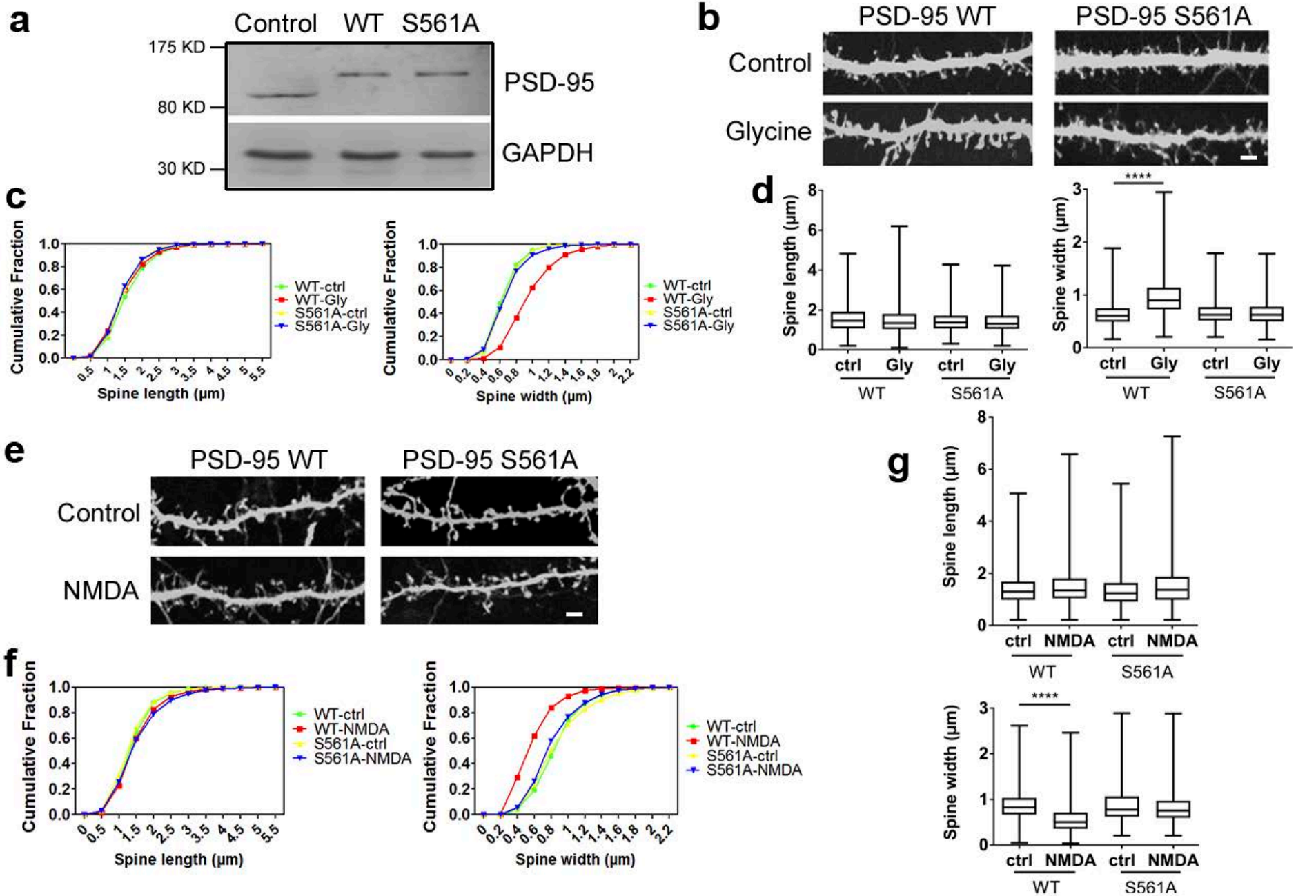

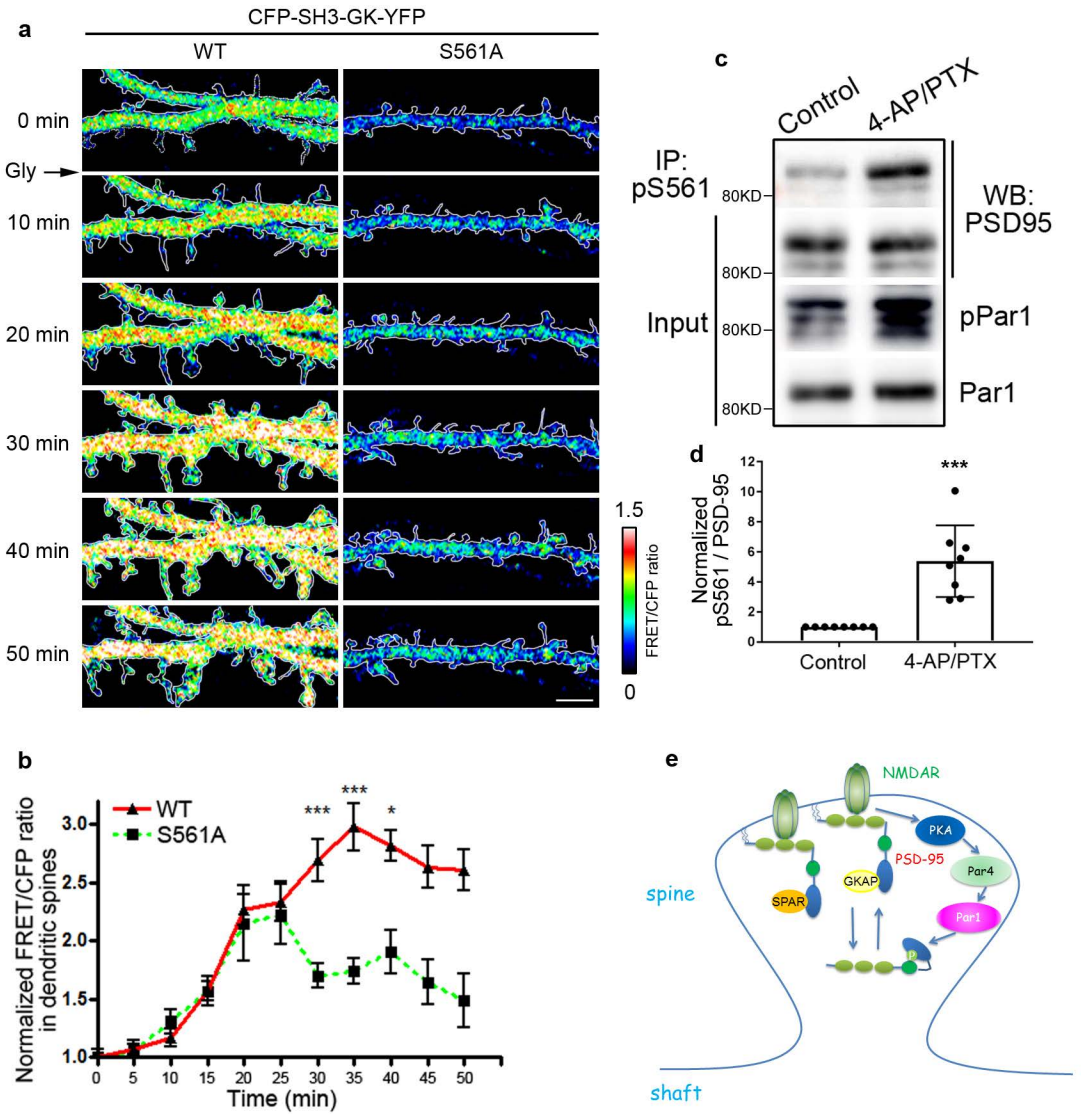
a
CFP-SH3-GK-YFP
WT
S561A
0 min
Gly
10 min
20 min
30 min
40 min
50 min
1.5
FRET/CFP ratio
0
b
WT
S561A
Normalized FRET/CFP ratio in dendritic spines
Time (min)
***
***
*
c
Control
4-AP/PTX
IP: pS561
WB: PSD95
Input
pPar1
Par1
80KD
d
Normalized pS561 / PSD-95
***
Control
4-AP/PTX
e
NMDAR
PKA
PSD-95
Par4
GKAP
SPAR
Par1
spine
shaft

Postsynaptic density 95 (PSD-95) serine 561 phosphorylation regulates a conformational switch and bidirectional dendritic spine structural plasticity

Qian Wu, Miao Sun, Laura P. Bernard and Huaye Zhang

J. Biol. Chem. published online August 8, 2017